LA-UR 90-3542

CONF-9010209--3

Los Alamos National Laboratory is operated by the University of California for the United States Department of Energy under contract W-7405-ENG-36.

LA-UR--90-3542

DE91 001954

TITLE: A VIEW ON ADVANCES IN SPHEROMAK UNDERSTANDING AND PARAMETERS.

AUTHOR(S): J. C. Fernandez, R. E. Chrien, F. J. Wysocki, R. M. Mayo, and I. Henins.

SUBMITTED TO: IEA Workshop on Physics of Alternative Magnetic Confinement Schemes, Villa Monastero, Varenna, ITALY (OCTOBER 15-24, 1990).

DISCLAIMER

Los Alamos Los Alamos National Laboratory
Los Alamos, New Mexico 87545

October 8, 1990

A View on Advances in Spheromak Understanding and Parameters

J. C. Fernández, R. E. Chrien, F. J. Wysocki, R. M. Mayo, and I. Henins

Los Alamos National Laboratory, Los Alamos, NM 87545

A spheromak is a toroidally-shaped magnetized plasma configuration in which no material (such as coils or vacuum vessels) links the torus, so that the topology of the spheromak boundary is spherical. In the period since the properties of a nearly force-free ($\nabla \times \vec{B} \approx \lambda \vec{B}$) spheromak configuration were described using single-fluid MHD theory[M. N. Rosenbluth, M. N. Bussac, Nucl. Fusion **19**, 489 (1979)], and since the first spheromak was formed at the Univ. of Maryland [G. C. Goldenbaum *et al.*, Phys. Rev. Lett. **44**, 393 (1980)], remarkable theoretical and experimental advances have been made. This paper highlights some of that work. Some of the latest results from the CTX group at Los Alamos are also presented. These include the observation of suprathermal electrons in CTX, evidenced by X-ray bursts with photon energies above 1 MeV.

1. Theoretical Background

Magnetic equilibria in closed systems: Force-free states ($\vec{J} \parallel \vec{B}$) satisfy

$$\nabla \times \vec{B} = \lambda(\psi)\vec{B}, \tag{1}$$

where $\vec{J}$ and $\vec{B}$ are the current per unit area and magnetic field, and

$$\lambda(\psi) = \mu_0 \vec{J} \cdot \vec{B}/B^2 \tag{2}$$

is constant on magnetic flux surfaces (parametrized by a normalized flux function ψ). In nearly force-free magnetohydrodynamic (MHD) equilibria, such as spheromaks and reversed-field pinches (RFP), it is useful to consider magnetic helicity, the linkage of magnetic flux within a closed boundary[1]. For times much shorter than the resistive diffusion time, helicity conservation has been

verified in spheromaks[2–4] and RFPs[5]. When the boundary of the system is a magnetic flux surface (for example, a volume bounded by a perfect conductor with no initial magnetic flux penetrating the wall), the helicity is given by

$$K = \int \vec{A} \cdot \vec{B}\, dvol, \tag{3}$$

where $\vec{A}$ is the vector potential. Helicity is a global quantity and helicity density is not a well defined concept. When the boundary is not a magnetic surface, Eq.(3) is not gauge invariant. Berger and Field[6] view the problem as arising from the indeterminacy of the flux linkage outside the volume of interest. Their solution is to substract the contribution from a reference field $\vec{P}$, such that $\nabla \times \vec{P} = 0$, $\vec{B} \cdot \hat{n} = \vec{P} \cdot \hat{n}$, and $d(\vec{B} \cdot \hat{n})/dt = d(\vec{P} \cdot \hat{n})/dt$. ($\hat{n}$ is the unit vector normal to the surface.) The resulting generalized helicity[6], which reduces to Eq.(3) when the boundary is a magnetic surface, solves the gauge problem. (K denotes hereinafter the generalized helicity.) For spatially constant λ,

$$2\mu_0 W/K = \lambda \tag{4}$$

where $W = \int B^2/2\mu_0\, dvol$ is the magnetic energy. Of the possible Woltjer-Taylor (constant λ) states[7–11], one has minimum magnetic energy per unit helicity at a value $\lambda = \lambda_{me}$ dependent on the system geometry. (In an equilibrium with non spatially constant λ (Sec.3), $2\mu_0 W/K = \langle\lambda\rangle$, where the weighted eigenvalue $\langle\lambda\rangle$ is in practice very close to λ_{me}.) λ can also be considered as the inverse of the characteristic size of the system. In a geometry consisting of coupled subvolumes of different shapes, the equilibrium expands into the region of largest characteristic size, minimizing its magnetic energy per unit helicity[12].

In a cylinder of length L and radius a, with vanishing radial magnetic field at the walls, no net flux, and assuming a spatially constant λ, $\vec{B}$ in Eq.(1) has analytic solutions[13] involving the functions $J_m(\nu_k r)e^{i(m\theta - kz)}$ and $J_{m-1}(\nu_k r)e^{i(m\theta - kz)}$, where r, θ and z are the radial, azimuthal and axial coordinates, J_m are the Bessel functions of the first kind, and $\nu_k^2 = \lambda^2 - k^2$ is adjusted to fit the boundary conditions. For fixed λ, assuming λ and k are purely real, the solutions are a discrete set in m and k. Finn *et al.*[14] showed that in a conducting cylinder of radius a closed on both ends, the $m = 0$ is the minimum energy state if the cylinder length is less than $1.67a$, whereas the $m = 1$ is the minimum energy state for longer cylinders. For an infinite cylinder, the $m = 1$ state has $\lambda_{me,1}a = 3.112$, while the $m = 0$ state has $\lambda_{me,0}a = 3.832$.

The first spheromak ($m = 0$ state) was formed in the PS-1 device at the University of Maryland[15]. The $m = 1$ state (a double helix along L) was first

observed at Los Alamos, in what was later named the CTX device, in a copper cylinder with $a = 0.32$ m and $L = 1.2$ m[16]. The pitch of the double-helix was measured in the $m = 1$ helicity source experiment[12] also at Los Alamos.

The force-free spheromak magnetic field is composed of the sum of the field generated by the internal plasma currents plus a superimposed external field[17]. When the spheromak is confined by a metallic wall, the "external" field is generated by the wall image toroidal currents. (Outside the wall, the magnetic fields cancel out.) For example, in the minimum-energy spheromak in a conducting cylinder with equal radius and height, the ratio of toroidal/poloidal plasma currents is 0.55 while the ratio of wall/toroidal currents is 0.56

Externally coupled states: For externally coupled states[18,13] (still assuming spatially constant λ), in which finite magnetic flux and plasma currents cross the system boundary, the continuum of solutions in λ for each m and k are dependent on the boundary conditions. In an infinite cylinder, with no radial field at the wall, but with non-zero net axial flux ϕ_z, the locus of solutions to Eq.(1) determine the F-Θ curve[10], where $F = \pi a^2 B_z(a)/\phi_z$ is the normalized toroidal magnetic field at the wall and $\Theta = \pi a^2 \vec{B}_\theta(a)/\phi_z$ is a measure of the axial current. At low current, F is unity, and the fields are tokamak-like. As Θ increases, F monotonically decreases, and the equilibrium corresponds to that of an ultra-low-q tokamak. F crosses zero at $\Theta = 1.2$, where the fields resemble those of a stabilized z-pinch, or equivalently, a straight spheromak. At higher Θ, the toroidal field at the wall reverses, and the fields are RFP-like. Up to $\theta = 1.6$, the minimum energy state has $m = 0$ symmetry. Above 1.6, the $m = 1$ state has lower energy instead, and the RFP develops a helical kink distortion[8].

In spite of the good agreement between the spatially constant λ hypothesis with experimental observations, departures from this hypothesis have been routinely observed on spheromaks[19,20,3], the $m = 1$ helicity source experiment[12], as well as in the ZT-40M RFP[21]. These arise either from modifications to the current density profile (by spatial nonuniformities of current drive or electrical resistivity) or from finite gradients of the plasma pressure. Thus, the comparison of the observed magnetic structures to the theoretical results described above represents a starting point only. But experimental observations can be very well modeled numerically by using physically reasonable $\lambda(\psi)$ profiles which preserve the qualitative features of the minimum energy states (spheromaks, double-helix, RFP) described above.

Helicity injection: When magnetic fields penetrate the boundary, helicity can be injected into (or ejected from) the system. The total time derivative of the generalized helicity [22,6] can be conveniently expressed by the relation[23]

$$\frac{dK}{dt} = -2\int \vec{E}\cdot\vec{B}\; dvol + 2\int \vec{E}_v\cdot\vec{B}_v\; dvol, \tag{5}$$

or equivalently,

$$\frac{dK}{dt} = -2\int\oint \vec{E}\cdot d\vec{l}\; d\psi + 2\int\oint \vec{E}_v\cdot d\vec{l}\; d\psi. \tag{6}$$

The subscript v refers to the reference vacuum fields with the same $\vec{B}\cdot\hat{n}$ and $\vec{E}\times\hat{n}$ boundary conditions as when the plasma is present. In Eqs.(5) and (6), the first term is just the resistive dissipation of helicity within the plasma. The second term represents helicity injection. Often, as shown below in Sec.2, the structure of the vacuum fields is obvious, and the helicity injection rate is easily computed. A steady state (sustainment) can be achieved where the helicity dissipation by the plasma resistivity is balanced by helicity injection.

2. Formation and sustainment

Five different methods of spheromak formation have been used: the magnetized coaxial source[24–26], the combined θ and z pinches[15], the flux core[27], the conical θ-pinch[28], and the kinked z-pinch[29] ($m = 1$ source). Initial spheromak formation experiments (the z, θ-pinch at Maryland, and the coaxial sources at Los Alamos and Livermore) were conceived and executed as "fast" formation schemes. Formation occurred in a period similar to the Alvén transit time (requiring high electrical power), and the currents were carefully programmed to allow the necessary magnetic reconnection to take place. Even the then slower (magnetic reconnection timescales) flux core method was executed on the basis of detailed MHD calculations[27].

Since then, spheromak formation has been understood and improved on the basis of helicity balance. These plasma sources are also helicity sources (Eqs.(5) and (6)), and the helicity is injected and incorporated into the spheromak equilibrium in timescales much shorter than the resistive decay time[4,2]. Helicity balance in the CTX source-spheromak system has been verified[4]. Moreover, helicity injection has balanced the resistive helicity dissipation and sustained CTX spheromaks[30] with toroidal currents of up to 500 kA for a period much longer than the resistive helicity decay time[31]. (The sustainment period was limited by the available Volt-seconds in the capacitor bank.)

The generality of the helicity injection model, independent of formation details, has been firmly established. A coaxial gun ($m = 0$ symmetry) has sustained an equilibrium with $m = 1$ symmetry[16]. The coaxial gun has also sustained flipped spheromaks, in which the outer spheromak poloidal field cannot simply connect to the gun electrodes[4]. A source with $m = 1$ symmetry (kinked z-pinch) has sustained spheromaks ($m = 0$ symmetry)[12], also a case with no possible simple connection of the spheromak flux to the source electrodes.

Alfvén pioneered the injection of plasma rings produced by a magnetized coaxial gun into vessels with insulating walls to study astrophysical phenomena[32]. Wells injected "plasmoids", with helicity produced by a conical θ pinch, into a vessel with insulating walls[33]. These objects had the magnetic axis outside the wall, and thus are not spheromaks. However "flux amplification" (toroidal-poloidal flux conversion by relaxation processes) was observed[34].

Coaxial gun source: Fig.1 illustrates the coaxial-gun spheromak-formation method. The gun is connected to the spheromak flux conserver by a conducting cylinder called the entrance region. The source center electrode contains a solenoid which is energized prior to the discharge, to produce a magnetic flux ϕ_{src} which links the inner and outer electrodes (Fig.1a). Once a gas puff into the inter-electrode gap has diffused enough, a voltage V_{src} between the electrodes is applied. The gas breaks down, and a radial current I_{src} (current density $\vec{J}_{src}$) between the electrodes is established. This radial current produces an azimuthal magnetic flux (magnetic field $\vec{B}_\theta$). The linkage of the azimuthal flux (produced at a rate V_{src}), due to the radial current, with the initial solenoidal flux constitutes the helicity generated by the source. When the source current grows sufficiently, $\vec{J}_{src} \times \vec{B}_\theta$ exceeds the restoring force of ϕ_{src}, the equilibrium expands into the flux conserver and relaxes into a spheromak within a few microseconds (Fig.1b). More generally, the characteristic size of the driven equilibrium at the source is $1/\lambda_{src} = \phi_{src}/\mu_0 I_{src}$. When $1/\lambda_{src}$ decreases below the characteristic size of a possible equilibrium at the entrance region, the helicity flows "down-hill" in λ[12], and the energy is minimized by the establishment of a spheromak at the flux conserver, the volume of largest characteristic size. Once V_{src} is turned off, the spheromak disconnects from the source and decays resistively (Fig.1c).

The final spheromak helicity content can be predicted using Eq.(6). The first term (dissipation) can be represented by K/τ_K, where τ_K is a function of the plasma resistivity and λ. To compute the second term (injection), the reference vacuum magnetic field is the solenoidal field, and the reference electric field is

due to the voltage applied between the electrodes. The resulting electrostatic helicity injection rate is then $2V_{src}\phi_{src}$. This result is easily understood by noting that for two simply linked tubes of flux ϕ_1 and ϕ_2, the magnetic helicity is $K = 2\phi_1\phi_2$[1]. In the coaxial gun, V_{src} is the production rate of azimuthal flux, which is linked by the invariant solenoidal flux ϕ_{src}. More fundamental MHD modeling of coaxial guns has been done in Ref.[35].

Since clean (radiative losses not dominating power balance) sustained spheromaks have been obtained[36], current-carrying electrode-plasma contacts apparently are not an important technological hurdle. Coaxial guns could provide inexpensive current-drive for a fusion reactor based on the spheromak, the tokamak or the RFP. Helicity injection with a coaxial gun has been demonstrated in a tokamak[37], and a tokamak with start-up and current-drive provided exclusively by coaxial guns[38] is under construction at the Univ. of Washington. A spheromak reactor based on a coaxial gun has been designed[39].

Theta-z pinch: Fig.2 illustrates spheromak formation with combined θ and z pinches, by which the first spheromak was formed at the University of Maryland[15]. Starting with a static gas fill, an axial magnetic flux ϕ_{src} linking the electrodes is produced by the θ coil. A voltage V_{src} is connected across the axial electrodes, which ionizes the plasma and draws an axial current. The helicity injection rate into the vacuum tank is $2V_{src}\phi_{src}$. The current in the θ coil is reversed, and the reversed bias field pinches the plasma and trapped initial bias flux towards the axis. The axial fields reconnect, and the spheromak is formed. There are no measurements of how much reverse axial flux links the electrodes (which would decrease or even reverse the helicity injection rate).

Helicity can be generated mechanically by physically "twisting" magnetic flux tubes[40]. With the θ-z-pinch, predicting the spheromak helicity content (versus that outside of the separatrix) is complicated by toroidally counter-rotating plasma cells twisting the spheromak poloidal field, apparently enhancing the spheromak helicity, as observed in the PS-3.5 device at Maryland[41].

Maintaining the voltage between the z pinch electrodes would maintain helicity injection, provided the reverse bias was limited (to maintain net flux along the initial direction linking the electrodes). This configuration corresponds to the "Bumpy z-pinch"[42], successfully achieved by the group at the University of Tokyo[43] after replacing the z-pinch electrodes by opposing plasma guns.

Flux core: The formation method based on an annular flux core[27] operates on the magnetic reconnection timescale. The core, covered by a resistive metal liner to allow flux penetration, contains both a torcidal solenoid (TF coil) to provide an azimuthal field, and a multi-turn azimuthal coil (PF coil) to produce a poloidal field surrounding the core. The linkage of the poloidal and toroidal fluxes produced by the core are the basis for helicity injection in this scheme.

The helicity injection rate of the flux core is $2V_{src}\phi_{src}$, where ϕ_{src} is the flux produced by the PF coil, and $V_{src} = d\phi_{TF}/dt$. This method intends to avoid current-carrying contacts to the walls. However the flux core is not in practice a flux surface, negating the non-electrode advantage. In principle, proper programming of the TF coil allows precise control of the spheromak profiles. In practice, early during formation the profiles relax to the minimum-energy state[44–46]. Fig.3 shows the spheromak magnetic profile evolution in S-1.

Oscillating currents in the PF and TF coils in the flux core could be used for steady-state AC helicity injection into a spheromak[47], akin to the F-θ pumping technique in RFPs[48]. However (with the benefit of hindsight), because of instability of non line-tied spheromaks without a conducting wall (see Sec.4.1) and because of the relative technical difficulty of the flux core formation method, we believe it is unlikely that this scheme would be preferred for future devices.

Kinked z-pinch (m=1 source): This method uses z-pinch electrodes linked by axial flux, with its axis normal to the spheromak symmetry axis[29,12]. The experiment is shown in Fig.4. The basis for helicity injection is the linkage of the initial bias magnetic flux ϕ_{src} along the z-pinch axis with the flux due to the axial pinch current, driven by the voltage between the electrodes (the vacuum vessel is grounded, and the electrodes are biased to $\pm V_{src}$). The injection rate is $4V_{src}\phi_{src}$. Possible advantages of this method include a better coupling of the source with an $m = 1$ state in the entrance region (the minimum energy state for that subvolume), which could decrease the relaxation drive (and associated magnetic energy loss) in the entrance region. Also the source impedance turned out to be significantly higher[12], an attractive technological feature. The linear z-pinch could be replaced by a toroidal (electrodeless) z-pinch driven by a transformer. A possible disadvantage is the $m = 1$ structure in the entrance region intruding into the spheromak flux conserver and causing stochasticity[12].

3. Equilibrium

Spheromak magnetic field profiles were verified in early experiments by internal magnetic probe measurements[15,27,2,30], all showing the required signatures of poloidal field reversal at the magnetic axis, toroidal field reversal at the geometric axis, and similar toroidal and poloidal magnetic flux magnitudes. Fig.5 shows the profiles from the Beta II spheromak[2].

Spheromak equilibria can be computed whether the boundary is a conducting wall or an external bias magnetic field. Minimum-energy spheromak MHD equilibria have been solved analitically in spherical[49] and cylindrical[14,50] geometries. In other geometries, the equilibrium is found by solving the Grad-Shafranov equation, with the poloidal flux as a free parameter determining the absolute field strength of the equilibrium. In addition to the boundary conditions, either: $p(\psi)$ and $\phi(\psi)$; or $p(\psi)$ and $\lambda(\psi)$ must be specified (ψ is the normalized poloidal flux function, $p(\psi)$ is the pressure profile, and $\phi(\psi)$ is the normalized toroidal flux function). For the minimum-energy state ($p(\psi) = 0$ and $\lambda(\psi)$ =constant), if the boundary is chosen to be a magnetic flux surface, the geometry of the boundary determines the magnetic field profile.

Radiation-dominated spheromaks are not likely to deviate far from the minimum-energy state. In dirty plasmas, the Spitzer resistivity tends to be spatially constant. With rising electron temperature, the increase in Z_{eff} partially offsets the decrease from $T_e^{-3/2}$. It has been shown that a minimum-energy spheromak with uniform resistivity decays self-similarly with a decay time $\tau_{B^2} = \mu_0/2\eta\lambda^2$ and remains in that state without assistance from relaxation processes[51]. Moreover, a decaying spheromak with uniform resistivity evolves towards the minimum-energy state[52,53]. As expected, cold spheromak profiles are usually found to be very close to the minimum-energy state[51,2,46,28].

Spheromaks with warmer electrons and better impurity control[54,3,55] exhibit higher resistivity gradients, which cause the $\lambda(\psi)$ profile to deviate from the minimum-energy state. These deviations are also observed in RFPs[11]. Internal current-driven ideal kink modes are predicted[56,3] and observed[3,57] for sufficiently large deviations from $\lambda(\psi) = constant$ (see Sec.4.4.2). The high β (due to high plasma density) of PS spheromaks cause measurable deviations from the minimum-energy profiles[20].

In achieving clean spheromaks, internal magnetic-probe measurements are a liability. Fitting data from magnetic probes at the plasma boundary (or equivalently, the measurement of the induced currents in the conducting wall) to the

results from a Grad-Shafranov equilibrium solver has been successfully used to model CTX equilibria[3]. Although surface magnetic fields at the boundary do not uniquely determine the equilibrium, data from CTX mesh flux conservers (MFC) is well fitted by equilibria calculated from a physically reasonable linear $\lambda(\psi)$ function[3] given by $\lambda(\psi) = \bar{\lambda}[1 + \alpha(2\psi - 1)]$, where $\bar{\lambda} = \int \lambda(\psi)\, d\psi$ is the average $\lambda(\psi)$, usually very close to λ_{me}. Fig.6 illustrates the evolution of the $\lambda(\psi)$ slope α for a typical CTX large (0.67 m radius) MFC discharge. The current and the $\lambda(\psi)$ profiles are peaked on the outer flux surfaces during sustainment. The safety factor q near the magnetic axis reaches unity, and the n=1 kink mode is observed. When the helicity source is turned off, the current at the outer flux surfaces decays faster due to higher resistivity there, and the current profile becomes peaked at the magnetic axis. The q near the magnetic axis decreases to 1/2, and the n=2 kink mode becomes unstable. Sometimes, the n=3 mode is observed after further peaking. In spite of the seemingly large deviations of the $\lambda(\psi)$ profiles, the magnetic energy of these spheromaks is less than 10% above that of the minimum-energy state with the same magnetic helicity content[3].

4. Stability

4.1. External current-driven (tilt and shift) modes

These modes occur when the spheromak is bounded by a vertical field and there is no nearby conducting wall. (This case includes steady-state spheromaks inside a non-superconducting metallic wall.) A spheromak in a uniform bias magnetic field is unstable to the tilt[49], with a growth time of a few Alvén times[14,50,58–60]. In simple terms, the magnetic moment of the spheromak opposes the bias field and tends to flip[61]. The tilt in the presence of bias flux is a relaxation process which conserves helicity. Initially, the spheromak toroidal flux does not link the bias field (no contribution to helicity). The bias field nibbles away at the spheromak poloidal flux once it flips [59]. Finally the bias flux is trapped near the spheromak geometric axis. The linkage of toroidal flux with the combined bias and remaining spheromak poloidal fluxes yields the same initial helicity (if dissipation is small during the process).

If the bias field is made mirror-like with a high enough curvature index ($n_i > 1$, where $n_i \equiv (-r/B_z)(\partial B_z/\partial r)$), the tilt is stabilized. But the spheromak is then unstable to the horizontal shift mode, because the spheromak tends to move to regions of lower field[61]. For $n_i < 0$ the shift is stable (but the tilt is

not), and for $0 < n_i < 1$ both the tilt and the shift are unstable[61]. Thus, a steady state spheromak reactor appears to need feedback stabilization, but the presence of a conducting wall near the separatrix would decrease the needed response-time of the circuit to an acceptable level.

A conducting wall sufficiently close to the separatrix provides image currents which stabilize the tilt and shift modes[49,14,50,61], provided the spheromak is sufficiently oblate, as verified experimentally[25,2]. For both modes, these image currents have sizable components along the poloidal direction[61].

Stabilization of the tilt and shift has been attempted using passive coils rather than full conducting shells, partly because a conducting shell near the spheromak separatrix is incompatible with the flux-core and the traditional θ-z-pinch formation methods. Using a current loop model[61], it has been predicted that properly placed figure-8 coils can stabilize both modes simultaneously (for times short compared to the coils' L/R time) provided n_i is close to unity[62]. Besides the possible discrepancies in applying this model to spheromaks (low aspect-ratio tori), it is difficult with simple coil sets to maintain a uniform field index throughout the spheromak cross section. Maintaining an index above zero on ProtoS-1/C without interfering with the formation process was difficult[63].

Line tying slows the growth rate of the tilt mode[64]. But line tying alone cannot completely suppress the tilt[63] for realistic plasma parameters. Initial short-lifetime spheromak experiments, using various combinations of figure-8 coils, saddle coils, and resistive liners, sufficiently slowed the tilt and shift modes to prevent a catastrophic end to the plasma[65–67]. "Wagon wheel" and solid metal plates, tested in ProtoS-1/C, have been effective only to the extent that line-tying has been present (for example, a copper plate allows a much faster growth rate than a thin stainless-steel wall does)[63]. Tilt-limited spheromak lifetimes with these metal plates match the lifetimes in ProtoS-1/C with figure-8 and saddle coils[63], suggesting that early experiments with figure-8 and saddle coils benefited significantly from line-tying. "Wagon wheel" spokes connected poloidally outside of the ProtoS-1/C flux core significantly decreased the growth rate, but effectively acted like a conducting wall too far away from the separatrix to completely stabilize the tilt[63].

Stabilizing schemes other than a close-fitting conducting wall have not suppressed the tilt and shift modes in larger stationary spheromaks. With figure-8 coils, S-1 was grossly unstable with less than 10% of the spheromak poloidal flux linking the flux core[44]. Stability for long enough to study S-1 confinement has only been possible with a pair of non-connected conducting funnels placed

at the spheromak poles along the geometric axis[44]. Even if these methods were made to work, open field lines which intersect walls or a neutral gas fill are extremely detrimental to global spheromak energy confinement[36,68,69].

A stationary spheromak is not stable in the space between two long coaxial conducting cylinders (the $m = 1$ double helix has minimum-energy). However, metastable spheromaks have been accelerated in just that configuration, in a scheme where the spheromak acts like a moving armature in a coaxial rail gun[70]. The acceleration is due to the toroidal flux generated behind the spheromak by current flow axially along the center electrode, radially along the spheromak surface, and back axially along the outer electrode. Spheromak translation might allow tokamak plasma refueling by injecting spheromaks deep enough before the spheromak unravels in the tokamak magnetic fields[71], as demonstrated in the ENCORE tokamak[37].

4.2. Internal current-driven modes

These modes have been described in Sec.3. They typically saturate at amplitudes of about 10%[3], as predicted, with the plasma settling into a new equilibrium including the helical distortion from the mode[72]. With finite resistivity, since there are no singular current densities in the saturated state, no rapid reconnection processes are predicted such as those associated with sawteeth in tokamaks[72]. Although this is often true experimentally, sawteeth-like oscillations have been seen in sustained CTX spheromaks[31].

The non-uniform $\lambda(\psi)$ profile driving the kinks is induced either by the formation and sustainment process[45,3], or by the higher edge resistivity in decaying spheromaks[3]. These internal kinks are sometimes very damaging, and sometimes inconsequential. In detached S-1 spheromaks, a single n=2 kink event has destroyed energy confinement[73,74]. In decaying CTX discharges in the large MFC, the n=2 saturated kink mode degraded particle confinement[36]. In the 0.6 m radius solid flux conserver (SFC) in CTX, the best energy confinement times of any spheromak have been obtained in the presence of the usual $\delta B/B \approx 10\%$ saturated n=2 kink level at the wall. In the $m = 1$ source experiment, resonance between the $m = 0$ spheromak and a large $m = 1$ distortion probably resulted in significant stochasticity[12]. In high current-density spheromaks in the 0.3 m radius solid flux conserver (SSFC), there is apparently significant stochasticity arising from the interaction of the

saturated n=2 kink with toroidal distortions of the flux conserver[75], resulting in degraded confinement and τ_{B^2} (see Secs.5.3 and 5.1).

4.3. *Pressure-driven modes*

The spheromak volume-averaged beta-limit β_c given by the Mercier criterion in a spherical boundary is a very low 0.2%, while for oblate boundaries $\beta_c \approx 1\%$[49,76–78]. The reason is unfavorable curvature and low shear of the spheromak magnetic field.

Magnetic shear in spheromaks can be significantly increased. The presence of a sharp current and flux hole along the spheromak geometric axis can raise β_c to the 10–40% range [49,76,77,56]. Sufficiently peaked $\lambda(\psi)$ profiles can also raise β_c significantly above 2%[49,56,78]. Modifying the shape of a cylindrically symmetric wall to have a "bowtie"-shaped cross section can raise β_c to 3% for spheromaks in the minimum energy state, and higher for the outwardly peaked $\lambda(\psi)$ profiles typical with coaxial gun sustainment[79]. Fig.7 shows this configuration. Should current holes or $\lambda(\psi)$ profile control prove difficult, a bowtie-shaped flux conserver represents a simple way of achieving a very useful β, while retaining the engineering advantages of the spheromak concept.

For ideal interchange modes, the Mercier limit is probably a conservative limit. For small violations, the growth rates are so small that resistivity, viscosity and kinetic effects would probably dominate ideal MHD effects[77]. Resistive pressure-driven modes, a potential problem[49,56], have not been identified in spheromaks. Should pressure-driven modes represent the ultimate limit to spheromak confinement, a "constant-β" scaling would result.

Initial spheromak experiments reported volume-averaged betas $\langle\beta\rangle_{vol}$ much above β_c, of up to tens of percent[15,27,65,66,20,80,54,81,82,44,83]. More recently in S-1, a local constant β scaling has been found at the magnetic axis[69]. But similarly to CTX spheromaks in the large MFC, the $\langle\beta\rangle_{vol}$ has decreased from previous values for reasons unrelated to pressure-driven modes[36,69]. The CTCC-II experiment at Osaka has obtained a $\langle\beta\rangle_{vol}$ of a few percent[84]. But because of limiters, CTCC-II has a current hole[84], thus its β_c should be higher. CTX spheromaks in the high current density SSFC show no evidence of pressure-driven instability, even though $\langle\beta\rangle_{vol} \approx 5\%$[75].

In decaying CTX spheromaks in the SFC, a pressure-driven interchange mode has been directly observed[85]. Even though $\beta_c \approx 0.5\%$ when the instability occurred, the electron density and temperature (from Multipoint Thomson

scattering) and the assumption of equal electron and ion temperatures (substantiated by Doppler broadening measurements of OV[86]) yield an actual $\langle\beta\rangle_{vol} \approx 5\%$[85]. During the decay of these discharges, the electron pressure profile continually peaked, until, when a critical pressure gradient was reached, the interchange occurred. But the electron pressure gradients were so large that the critical gradient from the Mercier criterion (using the linear $\lambda(\psi)$ profile fit to the magnetic probe data) was exceeded by a factor of 20 by the electron pressure alone[85]. However, it has been found that the magnetic probe data fits even better a $\lambda(\psi)$ profile which is strongly peaked off-axis and which, by virtue of its much higher β_c, greatly reduces the discrepancy between the data and the Mercier limit. Fig.8 shows the SFC geometry. Fig.9 illustrates the nature of the instability. The magnetic diagnostics show no signature associated with the interchange, as expected for this type of mode.

5. Confinement

Because of the variety of spheromak formation schemes, it is traditional to compare spheromak confinement in the decaying phase, when the spheromak fields are not being sustained by helicity injection, the spheromak has mostly disconnected from the source, and the formation details should make little intrinsic difference. In this paper we follow that tradition.

In early spheromak experiments, the dominant plasma loss mechanism and the limit to plasma electron temperature was impurity radiation[65]. The Maryland and Princeton groups expected that, once their gross stability problems were solved with loosely fitting conductors or a conducting center rod, the relatively small plasma-wall contact area would result in excellent plasma confinement in their experiments[65]. Meanwhile, the CTX group at Los Alamos, realizing that impurity radiation was dominating energy transport, decided to switch to a 0.4 m radius flux conserver constructed out of a mesh of copper bars (SMFC), to minimize the wall surface area in contact with the plasma and to allow the rapid "pump-out" of impurities out of the plasma[54]. As explained in Secs.5.1 and 5.3, both strategies were fatally flawed because of the disastrous effects of open field lines in force-free concepts, much beyond those in other concepts. Only the group at Osaka used the combination of technologies that could significantly advance spheromak research in the short term: solid flux conservers and titanium gettering for impurity control[55].

These strategies of wall-contact minimization for a while appeared to be working. In the CTX SMFC, an electron temperature of 100 eV was achieved for the first time in any spheromak[54]. The power balance in the SMFC was dominated by power losses from particle convection[82]. In spite of the higher temperatures, no increase in energy confinement time (relative to previous results in solid flux conservers[80]) was obtained because of an increased helicity decay time[54]. These problems came to a dramatic focus with the large MFC in CTX. In spite of large increases in magnetic field and toroidal plasma current (up to 1 MA), along with similar plasma and current densities, the resistive decay time remained independent of the core electron temperature, the energy confinement time did not improve, and $\langle\beta\rangle_{vol}$ actually dropped as R^2[36]. Similar global confinement results were obtained in S-1[69].

In most spheromak experiments the steady state approximation

$$\tau_E = \frac{3}{2}\langle\beta\rangle_{vol}\ \tau_{B^2} \tag{7}$$

is valid. With Eq.(7) as a model, β and τ_{B^2} are discussed in Secs.5.1 and 5.2.

5.1. Helicity dissipation

In nearly force-free configurations, relaxation processes tend to dispose of magnetic energy while conserving magnetic helicity. Magnetic helicity K is dissipated ohmically (through electron collisional resistance). So we examine first the determinants of helicity dissipation. Without $\lambda(\psi)$ gradients, the magnetic energy W and K decay proportionately(Eq.(4)). If $\lambda(\psi)$ is non-uniform, then magnetic energy and helicity are not dissipated at the same rates, and relaxation activity is possible. This fact (and its consequences for transport) makes the behavior of force-free configurations unique.

Non-radiation-dominated spheromaks with significant fractions of open magnetic flux have helicity decay rates much higher than predicted by the volume-averaged Spitzer resistivity[36,69]. This is because the global plasma resistance is dominated by the electron-neutral collisions at the spheromak edge, rather than by the lower volume-averaged Spitzer resistivity[36,69]. This is discussed here using CTX spheromaks in the large MFC. Fig.10 shows a diagram of the large MFC along with the poloidal flux surfaces, determined by fitting wall-current measurements to the MHD equilibrium model[3] accounting for the discreteness and finite conductivity of the mesh copper bars[36,68]. Because of the competition of effects such as current peaking into and field diffusion

out of the flux conserver, the open fraction of poloidal flux remains a nearly constant 25% throughout the decay phase. The plasma in the open field lines leaves fast. Without refueling, a severe shortage of current carriers develops. If unchecked, the edge plasma currents would simply die out, and the spheromak would turn into a field-reversed configuration (FRC) with nearly only toroidal current. This configuration is so far from the minimum-energy state, that strong relaxation activity attempts to drive edge plasma currents. But since the edge becomes nearly an insulator, $\eta\vec{J}$ grows without bound. From Eq.(6), the helicity dissipation rate also grows and the spheromak quickly dies[68,36,80].

MFC spheromak lifetimes can be extended by refueling the edge with a background hydrogen fill[80]. In that case, the voltage on the open poloidal field lines is limited to the Paschen breakdown voltage for hydrogen[87]. This is indeed observed in the large MFC[36]. Fig.11 shows the good agreement between: (a) A plot of the observed E_{eff} (which is $\approx \eta\vec{J}$ at the edge, as determined from helicity balance), versus the electron density n_e (which is proportional to the neutral fill pressure[80]); and (b) The corresponding Paschen curve for breakdown of hydrogen[36]. A posteriori, the helicity dissipation in the open flux from the electron-neutral resistivity is enough to account for the total spheromak helicity dissipation, so that the dissipation from the Spitzer resistivity at the plasma core can be neglected to within experimental uncertainty[36]. Because of this, a plot of core electron temperature versus τ_{B^2} yields no correlation whatsoever in both CTX with the large MFC and S-1[36,69]. This model is similar to the edge-helicity-dissipation model pioneered in the HBTX RFP[23].

The ideal situation is not to need edge refueling, so that plasma resistance is dominated by Spitzer resistivity, with τ_{B^2} increasing as the plasma temperature increases. This has been achieved in decaying spheromaks in the CTX SFC (before the onset of the pressure-driven mode) by combining a low-field-error flux-conserver design with Ti gettering for impurity control[85,86]. Fig.12, a plot of τ_{B^2} versus central electron temperature in the SFC, shows for the first time in a spheromak a positive correlation between these quantities[86].

5.2. *Plasma beta*

Because the internal spheromak magnetic fields are mostly self-generated, a particular β value is much more useful than in other devices such as tokamaks and stellarators, where these fields are mostly generated by external coils. An important figure of merit is the engineering beta, $\beta_{eng} \equiv \langle p \rangle_{vol} / B^2_{wall}$, where p is

the plasma pressure. Whereas in a tokamak $\beta_{eng}/\langle\beta\rangle_{vol} \approx 1$, in a spheromak the typical ratio is in the 3–4 range[80]. Thus a $\langle\beta\rangle_{vol} \approx 5 - 10\%$ in a spheromak yields an excellent β_{eng} as far as reactor design is concerned.

Presently, the most important issue in spheromak confinement research is understanding what determines the β limit. From the results in the CTX SFC (Sec.4.3), there is a limit beyond which excessively peaked plasma pressure profiles end catastrophically [85]. Higher order saturated modes could enhance energy transport, which might account for the constant-β-scaling observed in the core of the S-1 plasma[88]. In the CTX SFC, where (before the interchange) radiation dominates the energy transport as the plasma heats up, there is no evidence of such mode-induced transport[86]. In future experiments, resistive modes might become more important than ideal modes.

5.3. *Power balance with large fraction of open flux*

The deleterious effects of field-errors on confinement have been observed in both the S-1 and CTX experiments[36,69]. This operating regime does not represent a favorable confinement scaling for future experiments.

As discussed in Sec.5.1, helicity dissipation in open field lines can be limited by providing a neutral gas fill pressure. Even so, the results with a large open-flux fraction are not satisfactory. Because of parallel heat conduction, the electron temperature in these open flux surfaces is low, allowing deep penetration of the neutral hydrogen used for refueling. Although the mean free for neutrals into these plasmas is only a few cm, the process of multiple charge exchange is important[69] according to simulations for S-1 and CTX parameters. In this process, a cold neutral exchanges with a warm ion in the edge, and the resulting warm neutral penetrates deep into the core. This effect raises the calculated ratio of neutral to electron densities from the 10^{-5} range (ignoring multiple exchanges) to the 10^{-2} range (when multiple exchanges are considered)[69]. This is disastrous for spheromaks dominated by field errors.

Because the ohmic dissipation rates for helicity and magnetic energy are $\dot{K} \propto \eta\vec{J}\cdot\vec{B}$ and $P_{ohm} \propto \eta\vec{J}\cdot\vec{J}$, the dissipation rates at a flux surface are[36]

$$2\mu_0 dP_{ohm} = \lambda(\psi)\ d\dot{K} \tag{8}$$

(although helicity cannot be treated locally, its dissipation rate can be). Because of the applicability of the edge dissipation model, the ratio of ohmic power to

helicity dissipation is[36]

$$\frac{P_{ohm}}{\dot{K}} \approx \frac{\lambda(0)}{\langle\lambda\rangle} \tag{9}$$

with $\dot{W} - P_{ohm}$ dissipated by relaxation ($\lambda(0)$ is the value at the edge).

As discussed in Sec.5.1, because of resistive decay of the edge currents, the ratio $\lambda(0)/\langle\lambda\rangle$ can become small (even under the linear λ profile model[3]). So the power going to relaxation becomes dominant. Similarly in RFPs, it has been found that the "modified" Bessel function λ profiles (where the current goes to zero steeply at the edge) fit the data best[21]. How well do modified-Bessel profiles fit CTX data is under study. With such profiles in the CTX large MFC, the relaxation/ohmic power ratio would have approached unity[68].

The magnetic power which goes into relaxation, presumably via fluctuations which move plasma, apparently goes into ion heating. In both S-1 and the CTX large MFC, Doppler impurity ion temperatures T_D of hundreds of eV are measured, with typically $T_D/T_e \approx 4$[68,69]. If the bulk ion temperature is indeed that high, the importance of charge exchange losses becomes apparent. Both a zero-dimensional analysis[36] and a one-dimensional analysis[69] indicate that charge exchange losses are both dominant and sufficient to explain the energy balance in both the CTX large MFC and S-1. In both machines, this regime results in very unfavorable global confinement scaling. At constant electron density n_e, it is observed: $\dot{I} = constant \longrightarrow \tau_K \propto I$ (in CTX[36] where I is the spheromak current, and where the fraction of open flux and spheromak size are constant), or $\tau_K \approx constant$ (in S-1, where the size and the open flux fraction vary); electron pressure $\langle n_e T_e\rangle_{vol} \propto J$; $\langle\beta\rangle_{vol} \propto 1/J$, and; τ_E independent of J (in CTX[36]) or $\tau_E \propto 1/J$ (in S-1[69]). Clearly, this is not the way to operate.

Even if charge-exchange losses could be decreased, the regime with a large fraction of open flux is not desirable. For example, in sustained spheromaks, where $\lambda(0)/\langle\lambda\rangle > 1$[3], the ohmic power dominates. However, parallel thermal conduction can dispose of the heat. The ideal way to operate a spheromak in steady state is with a helicity source maintaining the edge currents to avoid excessive relaxation activity (and possible associated enhanced transport), but with a source bias flux of less than 1% of the spheromak poloidal flux to reduce parallel heat losses to acceptable levels[39].

Field errors due to a mesh or loose-fitting wall are not the only problem. In the higher current density and electron temperature spheromaks in the CTX SSFC (with copper walls and no limiters), all the classic signatures of field errors (*e.g.*, linear current decay, higher Doppler ion than electron temperatures)

are observed when the saturated n=2 kink mode is active[75,89]. Because of fabrication errors, the cylindrical walls of the SSFC are not exactly round. Apparently, the resonance between the n=2 mode and the perturbation induced by the wall creates a sufficiently high fraction of stochastic magnetic flux. Because of peak electron temperatures of up to 400 eV[75] and thus lower core plasma resistivity, the tolerable open flux fraction is now less.

In both ProtoS-1/C and S-1, the particle diffusion coefficient has been measured using a spark discharge between carbon tips located near the spheromak magnetic axis[90,91,74]. In both devices $D_\perp \approx 5D_{Bohm}$ fits the results well[91,74]. These measured diffusion coefficients have been found to correlate with pressure gradients[74]. In addition, these coefficients, in the nearly constant electron density n_e discharges considered, are consistent with the expected scaling $\tau_p \propto 1/v_{i,th}$ (assuming $T_e \propto T_i$, where $v_{i,th}$ is the ion thermal speed) resulting from pressure-driven modes and the observed $n_eT_e \propto B^2$. However, the associated particle replacement power is negligible [69].

Even if the Bohm-like diffusion observed in S-1 is due to pressure-driven turbulence, the actual values measured might be more characteristic of S-1 than of the intrinsic confinement limit in spheromaks. For example, in the CTX SFC, there is no gas fill pressure, so the refueling of the core plasma presumably ceases when the source is turned off. Whereas $5D_{Bohm} \longrightarrow \tau_p \approx 400\mu$s particle confinement time of the core plasma, it is observed instead $\tau_p \approx 1.6$ ms[85].

5.4. Power balance with small fraction of open flux

As discussed in Sec.5.1, spheromaks in the CTX SFC are the closest so far to the ideal error-field-free spheromak. The observation of more normal Doppler ion temperatures $T_D/T_e \approx 1$ indicates that most of the magnetic power ohmically heats the electrons[86]. The positive correlation of τ_{B^2} with peak T_e also supports this picture[86]. As a result, the highest global energy confinement time in any spheromak, $\tau_E = 0.2$ ms, has been obtained. This achievement, along with the results of the HBTX-1B results without limiters[92], are the best illustration so far of the importance of the edge helicity-dissipation model in the design of experiments with nearly force-free equilibria.

Because of the strong (non-optimal) pressure peaking observed in the CTX SFC[85], $\tau_{B^2} \propto T_e$ is obtained for the decay time[86], which yields $\tau_E \propto \beta T_e$. With a more gentle temperature profile where the globally-averaged electron temperature is proportional to the peak temperature, $\tau_{B^2} \propto T_e^{3/2}$ and $\tau_E \propto \beta T_e^{3/2}$

could be obtained. This yields: (at constant electron density n_e) $T_e \propto \beta I^2/R^2$ and $\tau_E \propto \beta^{5/2} I^3/R$, or; (at constant drift parameter $J/n_e\sqrt{T_e}$) $T_e \propto \beta^2 I^2$, $n_e \propto 1/\beta R^2$, $\tau_E \propto \beta^4 I^3 R^2$ and $n_e \tau_E \propto \beta^3 I^3$. Along with the high β_{eng} properties of the spheromak, these scalings illustrate the attractiveness of the concept.

As mentioned in Sec.5.3, confinement in the CTX SSFC is degraded late during decaying clean discharges, when the n=2 kink is strongly active. However there is often a period $\approx$ 100 μs after the gun is turned off when the amplitudes of both the n=1 and n=2 kinks are small, confinement is best and helicity dissipation is smallest[75,89]. Near this time in both clean and dirty discharges, in both He and deuterium, 1–3 bursts of hard X-rays, of up to 100 μs duration, are often observed with plastic scintillator and Ge pulse-height detectors. Simultaneous measurements with one scintillator looking through a glass window and another looking through the 1.25 cm-thick stainless steel vacuum tank indicate an attenuation of only 50% through the wall. Thus there is a significant flux above 1 MeV. The Ge detector sometimes detects precursor 50 keV–1 MeV photons. Sometimes, only these photons are observed (without a scintillator signal). Two scintillators displaced 90° azimuthally (both looking through the vacuum wall) indicate toroidally asymmetric hard X-ray emission. Less intense hard X-ray photons or even bursts are observed during sustainment (sometimes at regular intervals), and less frequently later during decay (even close to the end of the discharge).

These hard X-ray bursts, if originating from electrons accelerated by the loop voltage and finally hitting the wall, indicate good plasma confinement. With the $\approx$ 125 V loop voltage, a 10 km long field line and $\approx$ 40 μs are needed to accelerate electrons to 1 MeV. The lack of correlation with MHD activity indicate against instability electric fields being the source of electron acceleration. It is not known whether the source of the seed electrons is the gun or the spheromak plasma itself.

Acknowledgments: The spheromak review paper by Thomas Jarboe (in preparation) provided a unique perspective and a wealth of references from the literature on spheromaks. The spheromak and RFP bibliography databases compiled and maintained by Cris Barnes and Glen Wurden, respectively, have been invaluable in the preparation of this and many previous manuscripts. Useful discussions with Cris Barnes on runaway electrons are gratefully acknowledged. This work is supported by the US Department of Energy.

References

[1] Moffat, H. K., *Magnetic Field Generation in Electrically Conducting Fluids*, Cambridge University Press, New York, 1978.

[2] Turner, W. C. et al., Physics of Fluids **26** (1983) 1965.

[3] Knox, S. O. et al., Physical Review Letters **56** (1986) 842.

[4] Barnes, C. W. et al., Physics of Fluids **29** (1986) 3415.

[5] Schoenberg, K. F. et al., Physics of Fluids **27** (1984) 1671.

[6] Berger, M. A. and Field, G. B., Journal of Fluid Mechanics **147** (1984) 133.

[7] Woltjer, L., Proc. of the National Acad. of Sciences, USA **44** (1958) 489.

[8] Taylor, J. B., Physical Review Letters **33** (1974) 1139.

[9] Taylor, J. B., Relaxation of toroidal discharges to stable states and generation of reversed magnetic fields, in *Plasma Physics and Controlled Nuclear Fusion Research, 1974*, volume I, page 161, IAEA, Vienna, 1975, Proc. Vth International Conference, Tokyo.

[10] Taylor, J. B., Relaxation of toroidal discharges, in *Pulsed High Beta Plasmas*, ed. by Evans, D. E., p. 59, Pergamon Press, New York, 1976.

[11] Taylor, J. B., Reviews of Modern Physics **58** (1986) 741.

[12] Fernández, J. C. et al., Physics of Fluids B **1** (1989) 1254.

[13] Schaffer, M. J., Physics of Fluids **30** (1987) 160.

[14] Finn, J. M. et al., Physics of Fluids **24** (1981) 1336.

[15] Goldenbaum, G. C. et al., Physical Review Letters **44** (1980) 393.

[16] Jarboe, T. R. et al., Physical Review Letters **45** (1980) 1264.

[17] Salingaros, N. A., Modern Physics Letters B **3** (1989) 1285.

[18] Turner, L., Physics of Fluids **27** (1984) 1677.

[19] An, Z. G. et al., Spheromak tilting instability: Experiment and theory, in *Plasma Physics and Controlled Nuclear Fusion Research, 1980*, volume I, page 493, IAEA, Vienna, 1980, Brussels Conference.

[20] Hart, G. W. et al., Physical Review Letters **51** (1983) 1558.

[21] Schoenberg, K. F. et al., Nuclear Fusion **22** (1982) 1433.

[22] Jensen, T. H. and Chu, M. S., Physics of Fluids **27** (1984) 2881.

[23] Jarboe, T. R. and Alper, B., Physics of Fluids **30** (1987) 1177.

[24] Turner, W. C. et al., Journal of Applied Physics **52** (1981) 175.

[25] Jarboe, T. R. et al., Production of field-reversed configurations with a magnetized coaxial plasma gun, in *Proceedings of the International Symposium on Physics in Open Ended Fusion Systems, Univ. of Tsukuba*, Tsukuba, Japan, 1980.

[26] Armstrong, W. T. et al., Compact toroid experiments and theory, in *Plasma Physics and Controlled Nuclear Fusion Research, 1980*, volume I, page 481, IAEA, Vienna, 1981, Brussels Conference.

[27] Yamada, M. et al., Physical Review Letters **46** (1981) 188.

[28] Kawai, K. et al., Physics of Fluids **30** (1987) 2561.

[29] Jarboe, T. R. et al., Comments in Plasma Physics and Controlled Fusion **9** (1985) 161.

[30] Jarboe, T. R. et al., Physical Review Letters **51** (1983) 39.

[31] Wright, B. L. et al., Helicity conservation and energy confinement in CTX spheromaks, in *Plasma Physics and Controlled Nuclear Fusion Research, 1986*, volume II, page 519, IAEA, Vienna, 1987, Kyoto Conference.

[32] Alfvén, H. et al., Journal of Nuclear Energy, Part C: Plasma Physics **1** (1960) 116.

[33] Wells, D. R., Physics of Fluids **5** (1962) 1016.

[34] Lindberg, L. and Jacobsen, C., Astrophysics Journal **133** (1961) 1043.

[35] Barnes, C. W. et al., Physics of Fluids B **2** (1990) 1871.

[36] Fernández, J. C. et al., Nuclear Fusion **28** (1988) 1555.

[37] Brown, M. R. and Bellan, P. M., Physical Review Letters **64** (1990) 2144.

[38] Jarboe, T. R., Fusion Technology **15** (1989) 7.

[39] Hagenson, R. L. and Krakowski, R. A., Fusion Technology **8** (1985) 1606.

[40] Barnes, D. C., Physics of Fluids **31** (1988) 2214.

[41] Barrow, B. and Goldenbaum, G. C., Phys. Review Letters **64** (1990) 1369.

[42] Jensen, T. H. and Chu, M. S., Journal of Plasma Physics **25** (1981) 459.

[43] Katsurai, M. et al., Experimental and theoretical studies on the magnetic configuration of bumpy-z-pinch/flux-core-spheromak, in *Proceedings of the 11th US-Japan Workshop on Compact Toroids*, page 138, Los Alamos, New Mexico 87545, USA, 1989, Los Alamos National Laboratory, #LA-11808-C, Held on November 8-9, 1989.

[44] Yamada, M., Nuclear Fusion **25** (1985) 1327.

[45] Janos, A. et al., Physics of Fluids **28** (1985) 3667.

[46] Hart, G. W. et al., Physics of Fluids **29** (1986) 1994.

[47] Janos, A. C. and Yamada, M., Fusion Technology **9** (1986) 58.

[48] Bevir, M. K. et al., Physics of Fluids **28** (1985) 1826.

[49] Rosenbluth, M. N. and Bussac, M. N., Nuclear Fusion **19** (1979) 489.

[50] Bondeson, A. et al., Physics of Fluids **24** (1981) 1682.

[51] Watanabe, K. et al., Journal of the Phys. Soc. of Japan **50** (1981) 1823.

[52] Katayama, K. and Katsurai, M., Physics of Fluids **29** (1986) 1939.

[53] Sgro, A. et al., Physics of Fluids **30** (1987) 3219.

[54] Jarboe, T. R. et al., Physics of Fluids **27** (1984) 13.

[55] Uyama, T. et al., Nuclear Fusion **27** (1987) 799.

[56] Jardin, S. C., Nuclear Fusion **22** (1982) 629.

[57] Satomi, N. et al., Confinement experiments and simulation on the CTCC-I spheromak, in *Plasma Physics and Controlled Nuclear Fusion Research, 1986*, volume II, page 529, IAEA, Vienna, 1987, Kyoto Conference.

[58] Sato, T. and Hayashi, T., Physical Review Letters **50** (1983) 38.

[59] Hayashi, T. and Sato, T., Physics of Fluids **28** (1985) 3654.

[60] Mikić, Z. and Morse, E. C., Physics of Fluids **30** (1987) 2806.

[61] Jardin, S. C. et al., Nuclear Fusion **21** (1981) 1203.

[62] Jardin, S. and Christensen, U., Nuclear Fusion **21** (1981) 1665.

[63] Wysocki, F. J., Physics of Fluids **30** (1987) 482.

[64] Finn, J. M. and Reiman, A., Physics of Fluids **25** (1982) 116.

[65] Yamada, M. et al., Experimental investigation of the spheromak configuration, in *Plasma Physics and Controlled Nuclear Fusion Research, 1982*, volume 2, page 265, IAEA, Vienna, 1983, Baltimore Conference.

[66] Bruhns, H. et al., Physics of Fluids **26** (1983) 1616.

[67] Munson, C. et al., Physics of Fluids **28** (1985) 1525.

[68] Fernández, J. C. et al., Nuclear Fusion **30** (1990) 67.

[69] Mayo, R. M. et al., Physics of Fluids B **2** (1990) 115.

[70] Hammer, J. H. et al., Physical Review Letters **61** (1988) 2843.

[71] Perkins, L. J. et al., Nuclear Fusion **28** (1988) 1365.

[72] Park, W. and Jardin, S. C., Physics of Fluids **26** (1983) 1871.

[73] Ono, Y. et al., Physical Review Letters **61** (1988) 2847.

[74] Mayo, R. M. et al., Nuclear Fusion **29** (1989) 1493.

[75] Wysocki, F. J. et al., Progress with small, high-magnetic-field spheromaks in CTX, in *Proceedings of the 11th US-Japan Workshop on Compact Toroids*, page 185, Los Alamos, New Mexico 87545, USA, 1989, Los Alamos National Laboratory, #LA-11808-C, Held on November 8-9, 1989.

[76] Okabayashi, M. and Todd, A., Nuclear Fusion **20** (1980) 571.

[77] Gautier, P. et al., Nuclear Fusion **21** (1981) 1399.

[78] Mayo, R. M. and Marklin, G. J., Physics of Fluids **31** (1988) 1812.

[79] Marklin, G. J., MHD stable high beta spheromak equilibrium, in *Proceedings of the 11th US-Japan Workshop on Compact Toroids*, page 181, Los Alamos, New Mexico 87545, USA, 1989, Los Alamos National Laboratory, #LA-11808-C, Held on November 8-9, 1989.

[80] Barnes, C. W. et al., Nuclear Fusion **24** (1984) 267.

[81] Jarboe, T. R. et al., Spheromak studies on CTX, in *Plasma Physics and Controlled Nuclear Fusion Research, 1984*, volume 2, page 501, IAEA, Vienna, 1985, London Conference.

[82] Barnes, C. W. et al., Nuclear Fusion **25** (1985) 1657.

[83] Sinman, S. and Sinman, A., Comparative analysis at SK/CG-1 machine for spheromak plasma heating, in *Conference on Controlled Fusion and Plasma Physics*, page 807, Venice, 1989, European Physical Society, Volume 13B, Part II (Venice Conference).

[84] Nishikawa, M. et al., Pressure effect on equilibrium configuration of CTCC-II spheromak, in *Proceedings of the 11th US-Japan Workshop on Compact Toroids*, page 156, Los Alamos, New Mexico 87545, USA, 1989, Los Alamos National Laboratory, #LA-11808-C, Held on Nov. 8-9, 1989.

[85] Wysocki, F. J. et al., Physical Review Letters **61** (1988) 2457.

[86] Wysocki, F. J. et al., Physical Review Letters **65** (1990) 40.

[87] Engel, A. V., *Ionized Gases*, Oxford University Press, Oxford, 1955.

[88] Yamada, M. et al., Investigation of confinement properties of spheromaks, in *Plasma Physics and Controlled Nuclear Fusion Research, 1988*, volume 2, page 539, IAEA, Vienna, 1989, Nice Conference.

[89] Fernández, J. C. et al., Bolometry, spectroscopy and doppler T_i measurements in high current density CTX spheromaks, in *Proceedings of the 11th US-Japan Workshop on Compact Toroids*, page 176, Los Alamos, New Mexico 87545, USA, 1989, Los Alamos National Laboratory, #LA-11808-C, Held on November 8-9, 1989.

[90] Levinton, F. M. and Meyerhofer, D. D., Review of Scientific Instruments **58** (1987) 1393.

[91] Meyerhofer, D. D. et al., Physical Review Letters **60** (1988) 933.

[92] Alper, B. et al., Plasma Phys. and Controlled Nucl. Fusion **30** (1988) 843.

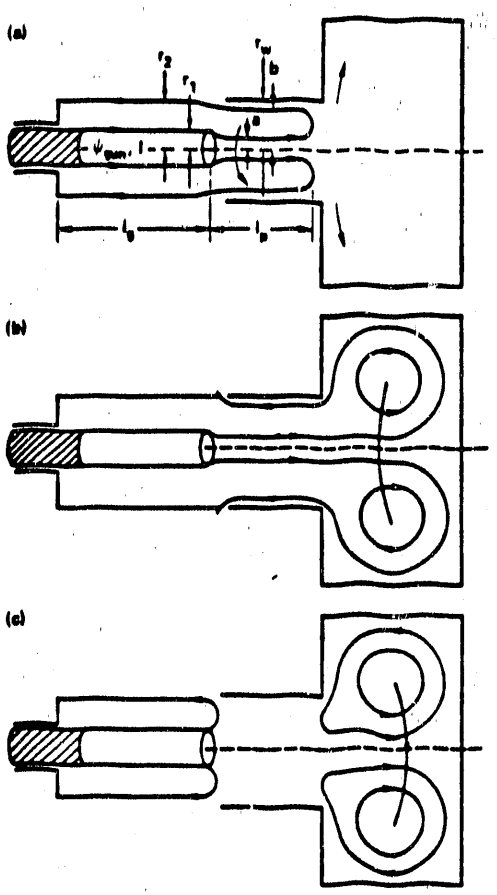

Figure 1: Spheromak formation by coaxial plasma gun[2].

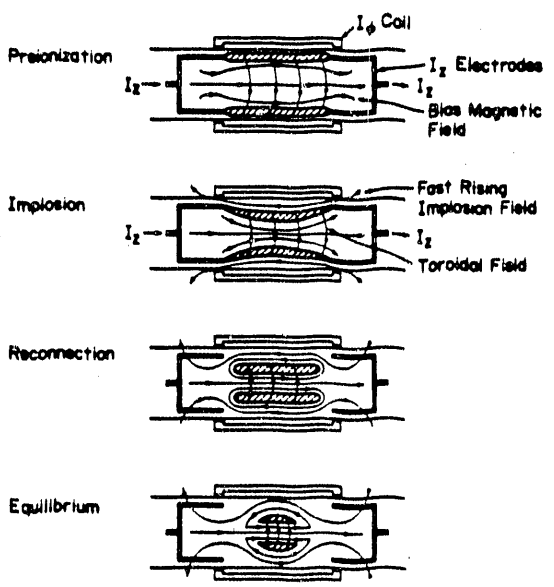

Figure 2: Spheromak formation by combined θ and z pinches[15].

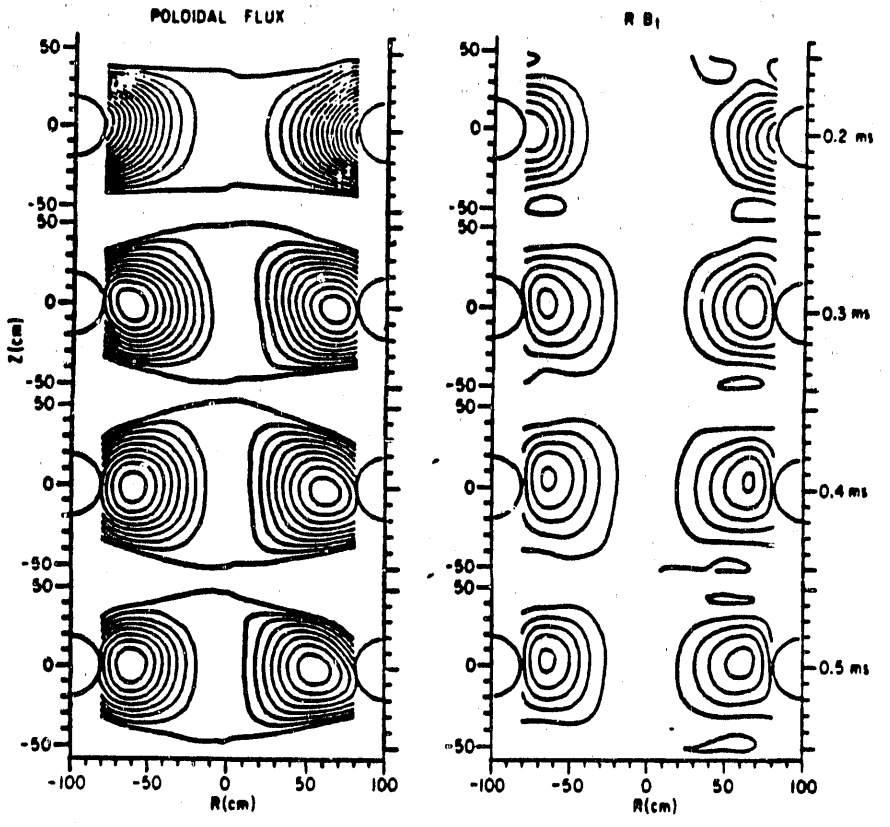

Figure 3: Poloidal and toroidal flux plots during S-1 spheromak formation obtained by internal magnetic probe data[45,44].

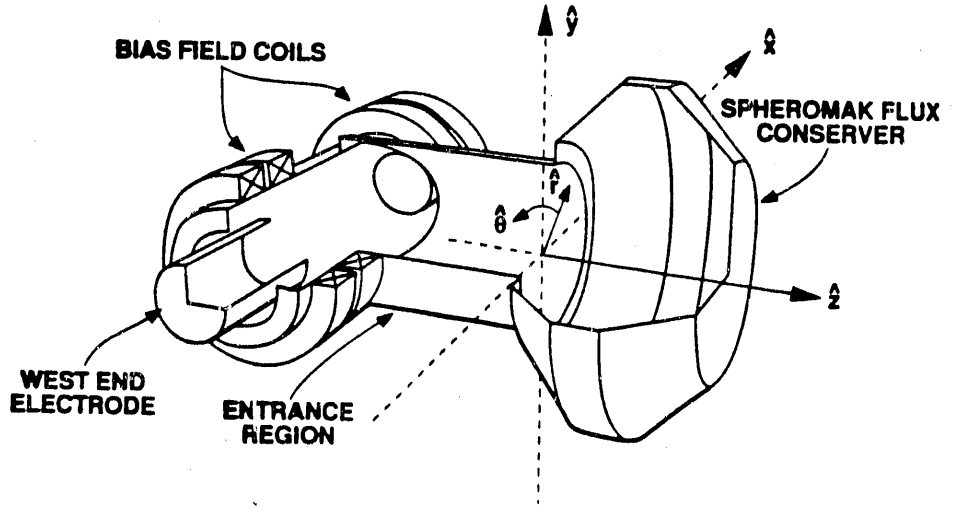

Figure 4: The $m = 1$ helicity source, entrance region, and spheromak flux conserver[12].

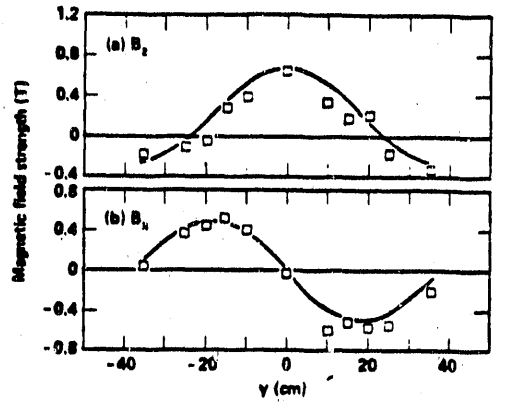

Figure 5: The measured poloidal and toroidal magnetic fields profiles in the Beta II spheromak compared to the profiles corresponding to the minimum-energy state[2].

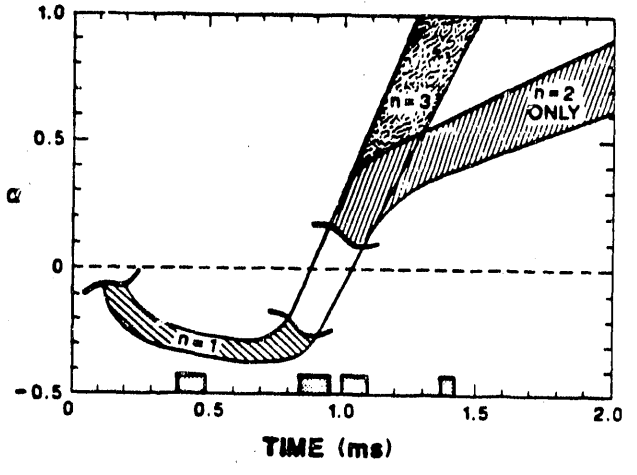

Figure 6: The measured evolution of the $\lambda(\psi)$ slope α for a typical CTX MFC discharge[3]. The shadowed regions indicate when the $\lambda(\psi)$ profiles deviate enough from the minimum-energy state ($\alpha = 0$) so that internal kink modes are observed, in good agreement with single-fluid MHD stability theory. The helicity source was turned off at 0.7 ms in these discharges.

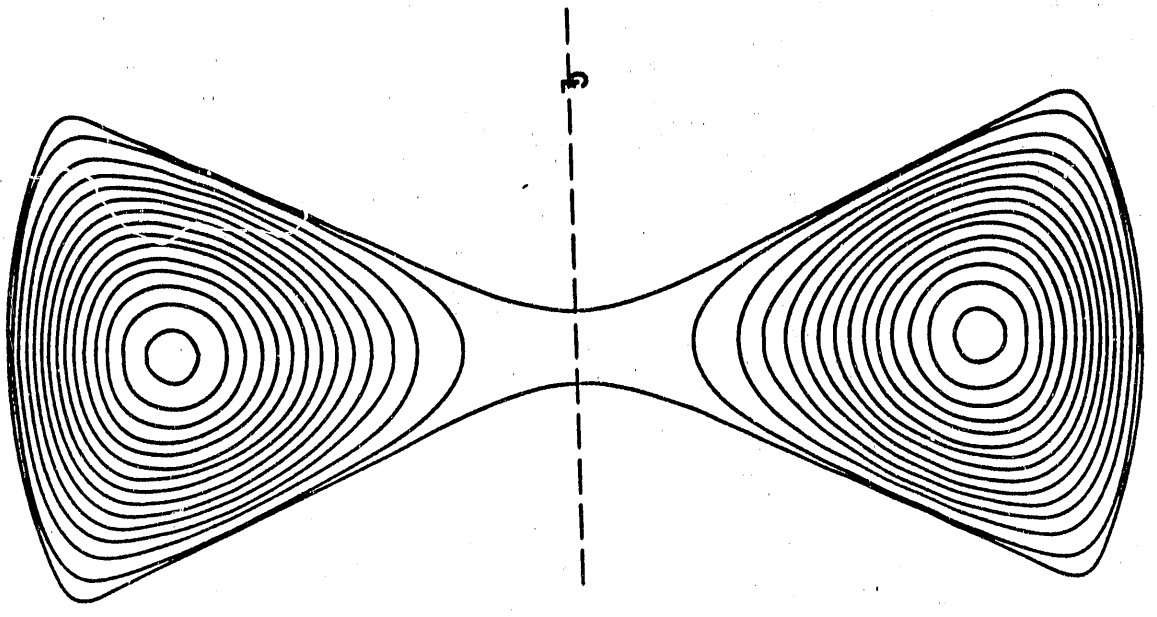

Figure 7: Cross section of the "bowtie"-shaped flux conserver, which results in a high magnetic shear equilibrium, significantly raising β_c[79].

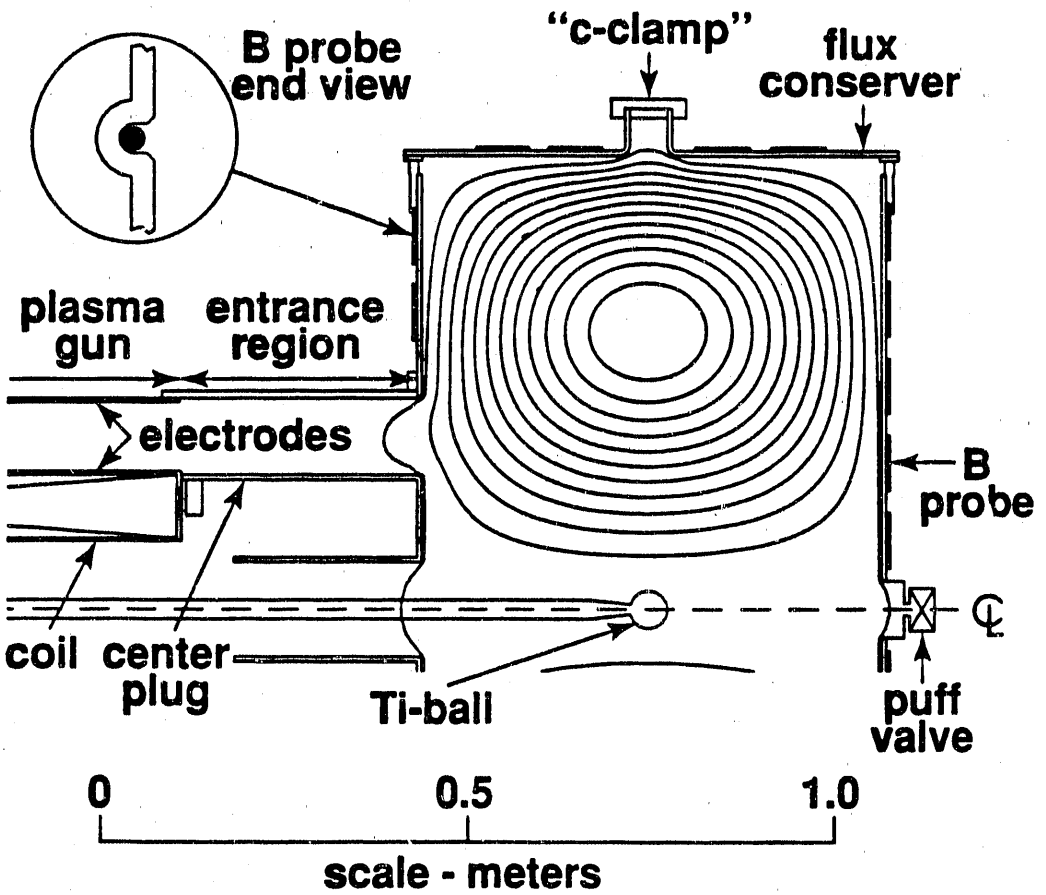

Figure 8: Geometry of the Solid Flux Conserver, entrance region and source in CTX. The poloidal flux surfaces, as calculated from the surface magnetic probe data fitted to the MHD equilibrium code results, are also shown. This flux conserver is specifically designed to minimize field errors (magnetic field penetration into the wall)[86].

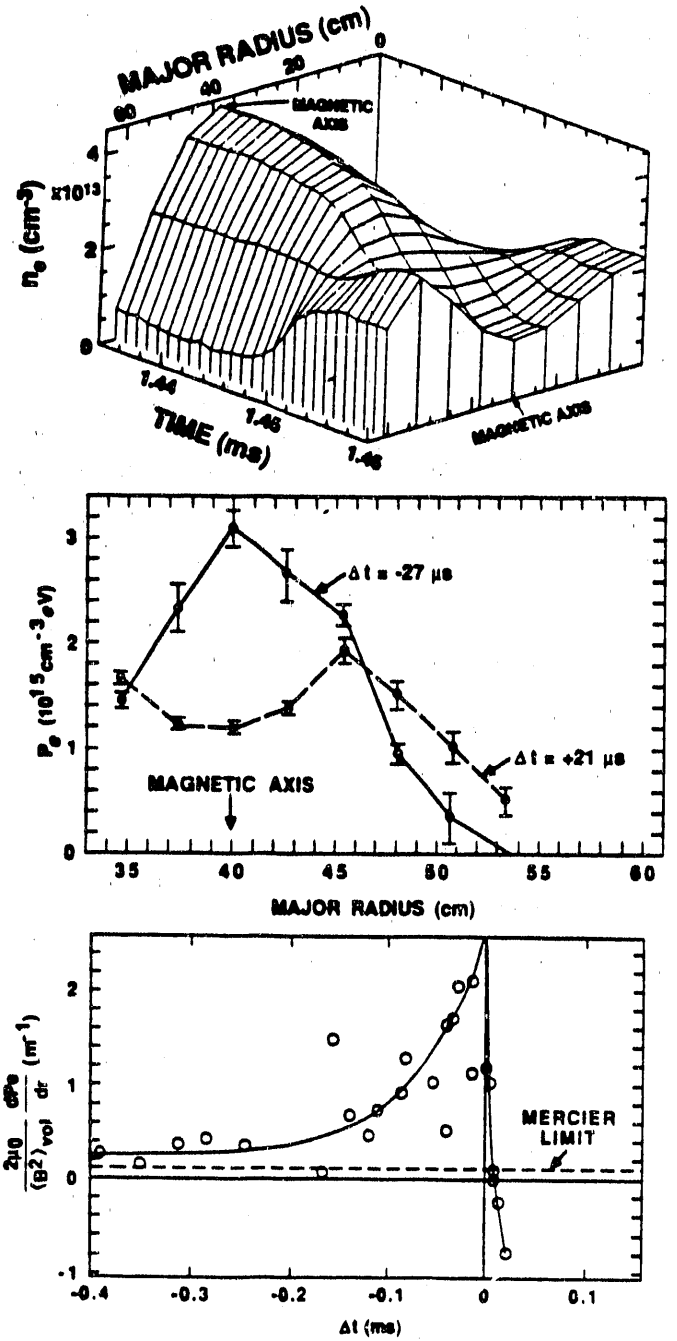

Figure 9: Pressure-driven instability in the CTX SFC. Top: Evidence for the interchange in the electron density profile, as reconstructed by from the eight-chord interferometer data; Middle: Evidence for the interchange on the electron pressure profile, as measured by the absolutely calibrated Thomson scattering diagnostic; and Bottom: Normalized electron pressure gradient increase versus time previous to the instability[85].

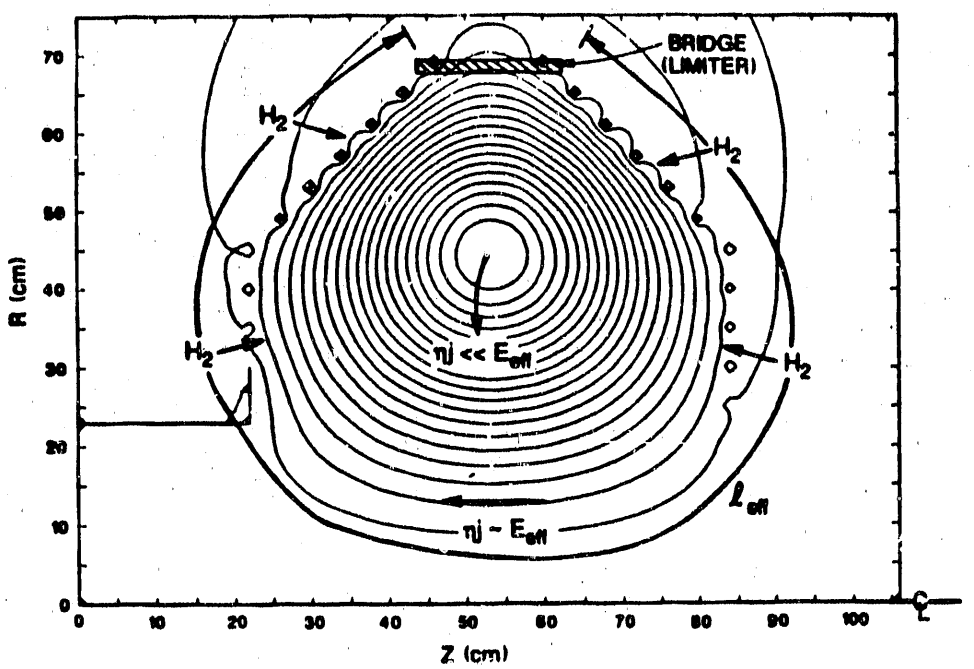

Figure 10: One-half of the CTX mesh flux conserver (MFC) cross section. Typical normalized spheromak poloidal flux contours (5% increments) during decay are included. The figure shows the typical 25% poloidal-flux fraction which intersects the wall during decay. In the figure, the poloidal field wraps around the magnetic axis in the counter-clockwise direction, while the toroidal field goes into the page. This corresponds to negative helicity ($\vec{J}$ antiparallel to $\vec{B}$)[68].

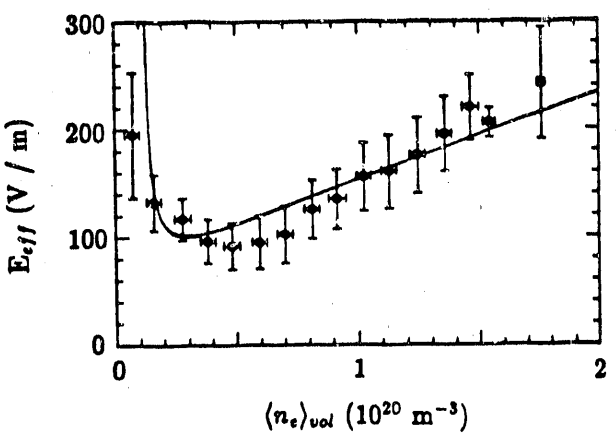

Figure 11: E_{eff} ($\approx \eta J_{||}$ at the edge) versus electron density for the CTX MFC. The 1825 data points are averaged in 20 intervals in density, with vertical error bars representing the standard deviation of the sample in each interval. The solid curve is the equivalent Paschen curve for breakdown in hydrogen corresponding to a 10 to 1 ratio of neutral to electron density (as observed experimentally in steady state), and a field-line length of l_{eff} =3 m (approximately the length of a field line at the edge)[36].

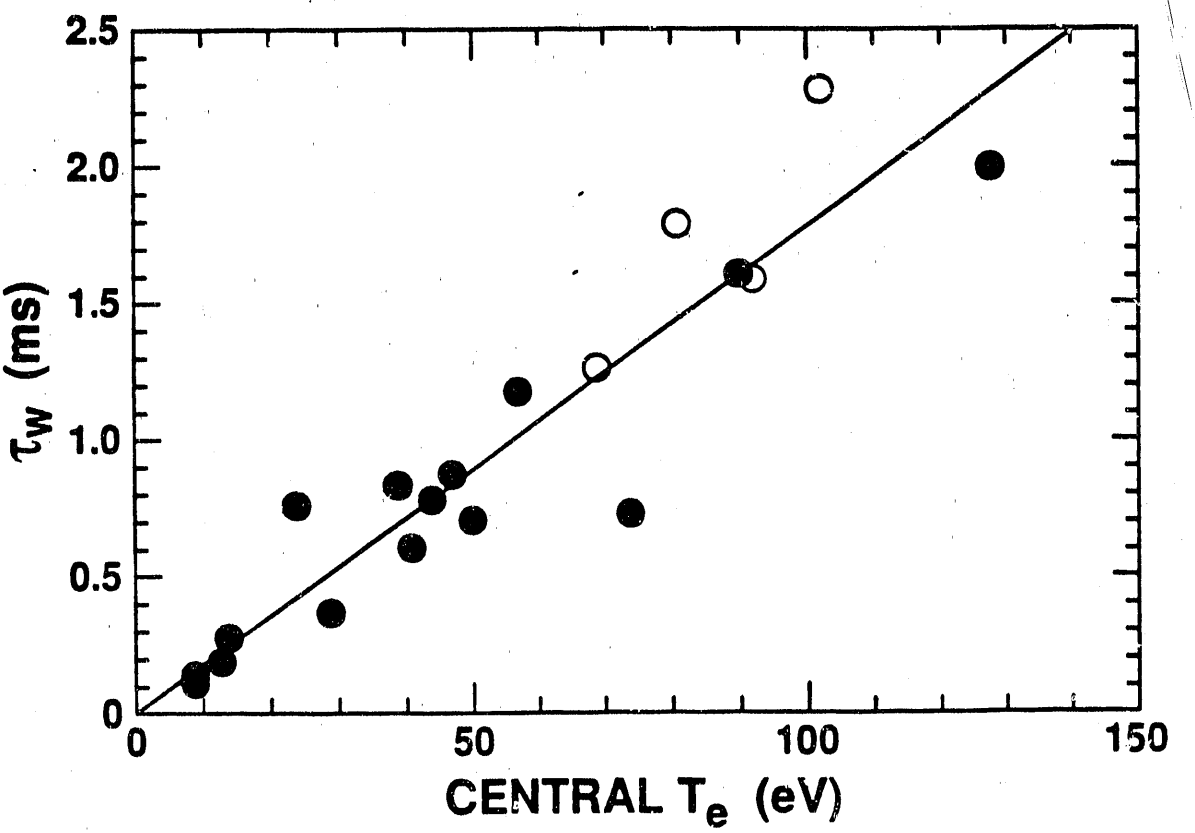

Figure 12: Plot of the magnetic energy decay time $\tau_W \equiv \tau_{B^2}$ versus central electron temperature in CTX spheromaks in the SFC. By using the electron temperature profile as determined from multi-point Thomson scattering, it has been determined that the decay rates in these discharges are consistent with the volume-averaged Spitzer resistivity with a $Z_{eff} \approx 2 \pm 1$[86].

END

DATE FILMED

11 / 26 / 90